Research Square

Preprints are preliminary reports that have not undergone peer review.
They should not be considered conclusive, used to inform clinical practice,
or referenced by the media as validated information.

Thermocapillary Bubble Oscillations and Migration in a Vibrating Cylinder in a Zero-Gravity Environment

Yousuf Alhendal (ya.alhendal@paaet.edu.com)
Public Authority for Applied Education and Training (PAAET)
Sara Touzani
Mohammadia School of Engineers, Mohammed V University in Rabat
Ali Turan
Abdelkhalek Cheddadi
Mohammadia School of Engineers, Mohammed V University in Rabat

Research Article

Keywords: Thermocapillary, Zero gravity, Bubble migration, Marangoni, Two-phase flow, Vibration.

Posted Date: October 10th, 2022

DOI: https://doi.org/10.21203/rs.3.rs-2113841/v1

License: This work is licensed under a Creative Commons Attribution 4.0 International License.
Read Full License

Abstract

Bubble migration in a vibrating zero gravity environment is numerically investigated using ANSYS-FLUENT software. A 3D CFD model is developed describing the two-phase flow of a nitrogen bubble immersed in a container full of ethanol. The Volume of Fluid (VOF) method and the geometric reconstruction scheme are used to track the liquid-liquid interface. The container is vibrated horizontally with different frequencies from 0 Hz to 1 Hz, and amplitudes from 0.005 m/s^2 to 0.1 m/s^2. The vibration impact on the bubble arrival times to the top and its ensuing dynamic is analyzed. Different bubble trajectory shapes are observed, other than the conventional vertical translation induced by the temperature difference. Compared to the no vibration case, the bubble motion is slightly either accelerated or decelerated for very low vibration amplitudes, A_b = 0.005 m/s^2. For a fixed frequency f = 1 Hz, the bubble arrival time increases significantly with the vibration amplitude increment relative to the no vibration case. The vibration effect becomes more intense with the Marangoni number decrease when f = 0.2 Hz and A_b = 0.005 m/s^2. Those results are difficult to obtain experimentally, signifying the importance of this numerical study to understand bubble motion and migration in space.

Introduction

Bubble motion inside a cavity has attracted researcher's attention for a long time, due to its importance in many industrial applications. From petroleum engineering to space, the formation of bubbles can sometimes be harmful for the enclosing equipment (cavitation issues) and beneficial when it is adopted to mass transfer operations [Thompson et al. (1980); Dijkink et al. (2006); and Nagasawa et al. (2001)]. When gravity is taken into account, bubble motion is complicated owing to bubble deformation, coalescence and break up. Many studies were performed regarding the dynamic behavior of a bubble and multiple bubbles [Krishna and Van Baten (1999); Radulescu and Robinson (2008); Yu et al. (2011); and Nie et al. (2015)]. By reason of buoyancy, thermocapillary force is negligible. In order to understand the influence of this force, previous studies investigated bubble motion in a microgravity environment including zero gravity conditions. Young et al. (1959) were the first to prove experimentally that a negative temperature gradient in the vertical direction in pure liquids is sufficient to hold small bubbles stationary or drive them downwards. Thus, the interfacial tension at the bubble surface will change with position because of its dependence on the temperature difference. This phenomenon is the thermocapillary migration. Subramanian (1992) discussed theoretically and experimentally thermocapillary motion of bubbles and drops. He confirmed the results obtained by Young et al. (1959) and showed that under certain conditions, a drop's pure thermocapilllary migration normal to a plane can be more rapid when the drop is near the surface than when it is far. Balasubramaniam et al. (1996) conducted experiments on isolated drop and bubble motion in a reduced gravity environment aboard the NASA Space Shuttle in orbit. They found quantitative discrepancies between the experimental results and the theoretical model of the migration velocity of air bubbles, but the qualitative tendency has been validated. The interaction between two drops was also examined. A small leading drop, with its motion unaffected, influences significantly the motion of a larger trailing drop by retarding it on account of the thermal wake behind the

leading drop. Furthermore, other experiments were carried out to extend the parameter range of this last experiment, Hadland et al. (1999), Wozniak et al. (2001). In Wozniak et al. (2001), the disturbance of the imposed temperature field through bubble motion is studied and compared to a theoretical model based on the numerical model developed by Ma et al. (1999), where the steady migration of a spherical drop is simulated in a liquid under zero gravity conditions. As a consequence of the complexity of the experiments and the disturbances that can occur, the results can sometimes be difficult to interpret. In order to circumvent those issues, many numerical models have been developed as a support for the onboard researches. Hermann et al. (2008) presented a numerical method to predict the thermocapillary motion of drops. It was found that the drop velocity decreases with Marangoni number (*Ma*) increase and the drops present a complex behavior at large *Ma* as observed by Wozniak et al. (2001). Using computational fluid dynamics (CFD) approach, Alhendal et al. (2013), analyzed a single bubble motion in stagnant fluid in 2D and 3D domains. Their results were in good agreement with the space experiments and showed that Volume of Fluid (VOF) method can be profitably employed to simulate thermocapillary flow.

Furthermore, after studying the bubble motion, other parameters were taken into consideration as the bubble size, shape and deformation [O'Shaughnessy and Robinson (2008); Colin et al.(2008); Nurse et al. (2013); Kalendar et al. (2021); and Wang et al. (2014)], the interaction between droplets [Alhendal et al. (2016 a); Balcazar et al. (2016) and Kalichetty et al. (2019)] and the drop behavior under rotation, [Yamagushi, et al. (2004); Gupta and Kumar (2007); and Alhendal et al. (2016 b)]. Another interesting factor is the influence of vibration on drop motion and behavior. It is well known that in spacecraft, while floating in a microgravity environment, vibrations occur classified as g-jitter. Managing those vibrations in space is crucial as an important tool to control flows and heat/mass transfers [Kawaji et al. (2006), Garrabos et al. (2007), and Ahadi and Saghir (2013)]. It is absolutely beneficial for different applications like crystal growth, fluid management, heat exchangers and multiphase flow. Therefore, even if theoretical studies were performed such as Bleich (1956), there is a still a lack of knowledge and understanding on vibration effects in a zerogravity environment. This complicated phenomenon intrigued many researchers and became a very focused topic. Movassat et al. (2009) studied numerically the interaction of two bubbles in a square vibrating container using the VOF solver. Their results showed that bubble collision occurs faster when the vibration frequency and amplitude are important. For high accelerations, bubble circular shape deforms, while only small shape oscillations are observed for small accelerations. At larger accelerations, bubbles breakup before their collision. Shoikhedbrod (2016) developed a model to prove that controlled vibration can be used to control gas bubble motion in the vertical direction and determine conditions of gas bubbles floating, drowning and oscillations in the liquid in reduced and microgravity environments. The theoretical and numerical results obtained were in good agreement with the parabolic aircraft tests.

By simulating complex behaviors such as Marangoni flows in zero gravity conditions using the CFD approach, we can in principle have a better understanding of the of the ensuing physical phenomena that occur in space and can subsequently manage it in the most optimum way possible. In this work, the

impact of vibration on the bubble motion and migration is investigated in a three-dimensional domain (3D) using ANSYS-FLUENT software.

Problem Statement

As shown in Fig. 1, the configuration studied is a cylindrical container filled with ethanol at a height of 120 mm and a diameter of 60 mm in a zero gravity environment. The upper and lower walls are held at temperatures T_{hot} = 330 K and T_{cold} =300 K respectively. The lateral walls are adiabatic. An isolated bubble of nitrogen N_2, with a diameter $d = 2\ r_b$, is placed in the middle of the container. Its behavior under the influence of the temperature difference and vibration is investigated in this 3D domain. The container is vibrated in the horizontal direction with different vibration amplitudes (A_b) and frequencies (f). No-slip condition is applied on all the walls. The bubble thermocapillary velocity is small and the flow is laminar. The host liquid is an incompressible Newtonian fluid and the thermophysical properties are assumed constant except for surface tension. Table 1 presents the physical properties of the host liquid and the gas bubble used in the simulations at T_0 = 300K.

Table 1
Physical properties used in the simulations for Ethanol and Nitrogen.

Properties	Ethanol	Nitrogen (N_2)	Unit
Density (ρ)	790	1.138	kg/m^3
Specific heat (C_p)	2470	1040.7	J/(kg.K)
Thermal conductivity (k)	0.182	0.0242	w/(m.K)
Viscosity (μ)	0.0012	1.66x10^{-5}	kg/(m.s)
Surface tension (σ_0)	0.0275	_	N/m
Surface tension coefficient (σ_T)	0.00009	_	N/(m.K)
Prandtl number (Pr)	16.28	0.79	_

As an initial condition, a steady state temperature field is established before releasing the bubble into the unsteady motion. The initial fluid velocity in the container is set to zero. The driving force for the flow is surface tension variation with temperature.

Mathematical Model

The migration velocity or the YGB model, based on the linear model of Young, Goldstein and Block 1959, is used to define the bubble velocity:

$$V_{YGB} = \frac{2\left|\frac{d\sigma}{dT}\right| r_b \lambda \frac{dT}{dx}}{(2\mu + 3\mu')(2\lambda + \lambda\prime)}$$

1

It is suitable for small Reynolds and Marangoni numbers defined respectively as:

$$Re_T = \frac{r_d V_T}{\nu}$$

2

$$Ma_T = \frac{r_d V_T}{\alpha} = Re_T . Pr$$

3

The Prandtl number is defined as the ratio of kinematic viscosity, υ, and thermal diffusivity, α.

$$Pr = \frac{\nu}{\alpha}$$

4

The velocity V_T derived from the tangential stress balance at the free surface is used to scale the migration velocity

$$V_T = \frac{\frac{d\sigma}{dT} . \frac{dT}{dx} . r_d}{\mu}$$

5

where $\mu$and μ', $\lambda and \lambda'$are the dynamic viscosity and thermal conductivity of continuous phase and gas, respectively. ρ is the density of the continuous phase fluid and$r_b$is the radius of the bubble. The constant $d\sigma/dT$or $\sigma_T$is the rate of change of interfacial tension and dT/dx is the temperature gradient imposed in the continuous phase fluid.

VOF model and Computational procedure:

In this study, ANSYS-FLUENT package is employed to solve the governing continuum conversation equations. It has been shown in Alhendal et al. (2013), that the use of volume of fluid (VOF) method is very suitable to track the liquid/ gas interface and solve two-phase problems. This method deals with completely separated phases without diffusion. The geometric construction scheme based on the piece-

wise linear interface calculation (PLIC) method of Young (1982) is chosen. Geo-reconstruction is an added module to the already existing VOF scheme that allows for a more accurate definition of the free surface, Hirt and Nichols (1981). The motion of the bubble–liquid interface is tracked based on the distribution of the bubble volume fraction, i.e. α_G, in a computational cell, where the value of α_G is 0 for the liquid phase and 1 for the bubble phase. Therefore, the bubble –liquid interface exists in the cell where α_G lies between 0 and 1.

Throughout the domain, a single momentum equation is solved and shared by all the phases, given below:

$$\frac{\partial}{\partial t}\left(\rho\overrightarrow{\nu}\right)+\nabla.\left(\rho\overrightarrow{\nu}\overrightarrow{\nu}\right)=-\nabla p+\nabla.\left[\mu(\nabla\overrightarrow{\nu}+\nabla\overrightarrow{\nu}^{T})\right]+\overrightarrow{F}+\overrightarrow{F}_{vib}$$

6

where $\overrightarrow{v}$ is treated as the mass-averaged variable:

$$\overrightarrow{v}=\frac{\alpha_G\rho_G\overrightarrow{v}_G+\alpha_L\rho_L\overrightarrow{v}_L}{\rho}$$

7

$\overrightarrow{F}_{vib}$ is the vibration force expressed as: $\overrightarrow{F}_{vib}=A_b sin(2\pi ft)$ (8)

and $\overrightarrow{F}$ represents volumetric forces at the interface, resulting from the surface tension force per unit volume. The continuum surface force (CSF) model proposed by Brackbill et al. (1992) is used to compute the surface tension force for the cells containing the bubble-host liquid interface:

$$\overrightarrow{F}=\sigma\frac{\rho kn}{\frac{1}{2}(\rho_L+\rho_G)}$$

9

where σ is the coefficient of surface tension,

$$\sigma=\sigma_0+\sigma_T(T_0-T)$$

10

and σ_0 is the surface tension at a reference temperature T_0, $T$is the liquid temperature, $\overrightarrow{n}$ is the surface normal which is estimated from the gradient of volume fraction, and k is the local surface curvature, given as:

$$k = -(\nabla \widehat{n}) = \frac{1}{\overrightarrow{n}}\left[\frac{\overrightarrow{n}}{|n|}\nabla |n| - (\nabla . \overrightarrow{n})\right]$$

11

The tracking of the interface between the bubble and host-liquid is accomplished by the solution of a continuity equation for the volume fraction of bubble:

$$\frac{\partial}{\partial t}(\alpha_G \rho_G) + \nabla \cdot \left(\alpha_G \rho_G \overrightarrow{v}_G\right) = 0$$

12

The volume fraction equation is not solved for the host-liquid; rather, the liquid volume fraction is computed based on the constraint:

$$\alpha_G + \alpha_L = 1$$

(13)

where α_G and α_L are the volume fraction of the bubble and host-liquid phases respectively. The transport equation properties are determined by the presence of the component phases in each control volume and are calculated as volume-averaged values. The density and viscosity of each cell at the interface is computed by the application of the following equations:

$$\rho = \alpha_G \rho_G + (1 - \alpha_G)\rho_L$$

14

$$\mu = \alpha_G \mu_G + (1 - \alpha_G)\mu_L$$

15

where ρ, μ and α_G are the density, viscosity and volume fraction of the different phases respectively.

The energy equation is also shared among the phases:

$$\frac{\partial}{\partial t}(\rho E) + \nabla . \left[\overrightarrow{\nu}\left(\rho E) + p\right)\right] = \nabla . (\kappa_{eff} \nabla T)$$

16

The VOF model treats energy (E) and temperature (T) as mass-averaged variables:

$$E = \sum_{q=1}^{n} \alpha_q \rho_q E_q \quad (17)$$

where Eq. 16, for each phase is based on the specific heat of that phase and the shared temperature. The properties ρ and k_{eff} (effective thermal conductivity) are also shared by the phases.

Numerical Resolution

After creating the geometry and the mesh, the finite volume grid obtained is transported into the Ansys-Fluent software. The calculations are carried out using the pressure-velocity formulation embodied in the PISO algorithm (Pressure-Implicit with Splitting of Operators) that performs two corrections on the grid quality related to cell neighbor and skewness. The pressure interpolation is achieved using a pressure-staggering option (PRESTO) scheme, while the momentum and the energy equations were discretised using a second-order upwind differencing scheme. Other algorithms were also tried, such as QUICK, instead of the second-order upwind scheme. Using these alternative methods gave similar simulation results. However, using non-iterative methods is generally faster than the use of iterative alternatives regarding computational time. Based on the simulation employing different operational conditions, convergence is generally obtained using a non-iterative time step of 5×10^{-3} s. All simulation runs are executed using double-precision accuracy and no gravitational force is imposed.

Model Validation

Nitrogen bubble was placed 10 mm from the bottom (cold) wall using the region adaptation setting on Ansys-Fluent (v.13, 2011). The size of the computational wall-bounded domain was chosen as 120 x 60 mm with impermeable sides (see Fig. 1). For simulations, the properties of nitrogen and ethanol were taken as those given in Table (1) from Thompson et al. (1980). The VOF model with the UDF were examined and validated properly. The results in Fig. 2 shows that the surface tension coefficient was well coded, suggesting that it is an appropriate choice to solve thermocapillary problems (Alhendal et al. (2013,2016)).As the accuracy of the simulation is mostly dependent on mesh density, the process of using different mesh sizes, time steps, convergence criteria and discretisation schemes, grid tests and extending the geometry to a fully three-dimensional model was all checked and grid independency was achieved by studying five different meshes as presented in Fig. 3 and Table 2. It has been found that a grid of 324000 nodes corresponding to 576 cells per bubble diameter is the most suitable mesh that gives good results with less computing time and memory usage, the results were also in good agreement with those found by Thompson et al. (1980), and Alhendal et al. (2017). In the present paper, the same grid is used for all the calculations. Figure 4 shows the 2D results for three different temperature gradients at time step = 5 s. As shown, the bubble absorbs heat at the front and rejects it at the cold end, as pointed by Nas & Tryggvason, 1993.

Table 2
Grid sensitivity check for a bubble with diameter of 10 mm for 3D models

Grid	(Δx,Δy)	Number of cells	Cells per bubble diameter	Bubble speed (m/s)
(1)	1.0 x 1.0	324000	576	0.0149
(2)	0.6 x 0.12	384800	680	0.0150
(3)	0.6 x 0.11	448000	780	0.0148
(4)	0.475 x 0.95	777216	1324	0.0148
(5)	0.45 x 0.8	889644	1556	0.0150

Results And Discussion

On earth, low frequencies 0 Hz $\leq f \leq$ 1 Hz are usually neglected. However, in space this range of vibration frequency can create oscillatory disturbances. At first, the vibration amplitude is fixed at A_b= 0.005 m/s^2 and the frequency impact on the bubble migration is discussed. The temperatures of the bottom and the top walls are held at T_{cold} = 300K and T_{hot} = 330 K respectively (Ma_T = 488). Then, for f = 1 Hz, the vibration amplitude is varied ranging from 0.005 m/s^2 to 0.1 m/s^2 and its effect is analyzed on the bubble dynamics.

Vibration Frequency

For Ma_T = 488 and A_b = 0.005 m/s^2, the effect of vibration frequency on the bubble motion is plotted in Fig. 5. When the vibration is absent, the bubble moves in a vertical trajectory from the container bottom to its top. At f = 0.01 Hz, a vertical translation of the bubble is observed at first. Then, in a position, almost equal to the half of the container height, the bubble motion deviates slightly to the left and continues deviating until it arrives at the top. A similar behavior is observed for f = 0.05Hz with an enhancement of the trajectory deviation from a position before the half of the container height, near the bottom. The bubble arrives at the top in a position far from the center. By increasing f to 0.1 Hz, the bubble oscillates creating a trajectory in the shape of a snake and reaches the top almost in the center. For f = 0.175 Hz, the bubble trajectory becomes undulated and the bubble breaks up when it reaches the top. When the frequency is much important (f = 1 Hz), the bubble motion seems to be in a vertical translation, however, this is not the case. The bubble oscillates periodically around the container vertical axis until it arrives at the top. Figure 6 shows the bubble center position in the three directions. For no vibration case and all the frequencies, the bubble travels from the bottom to the top (Y direction) similarly in the first 2.5s, then, beyond 2.5s, the bubble arrives rapidly at the container top when f = 0.175 Hz and f = 1 Hz taking 10.75s (Fig. 6a). This time is reduced by 0.25s, 0.5s and 0.75s vis-à-vis the no vibration case, f = 0.01 Hz, and both f = 0.05 Hz and f = 0.1 Hz respectively. This slight difference in the arrival time can be explained by

the oscillatory movements observed in both the X and Z directions (Fig. 6b and 6c). Those pulsations deform the bubble shape from its initial circular shape as observed by Movassat et al. (2009). Therefore, the shape change affects the bubble motion. In general, the primary force influencing the motion is thermocapillary, but choosing the right frequency can accelerate the bubble migration. For f = 0.01 Hz, f = 0.05 Hz and f = 0.1 Hz, the bubble migration is delayed compared to the no vibration case. The deviation of the bubble from the center reduced the bubble motion.

Vibration Amplitude

In this section, for Ma_T =488, the vibration frequency is fixed at f = 1 Hz and its amplitude, A_b, is varied ranging from 0.005 m/s^2 to 0.1 m/s^2. Actually, the bubble motion becomes complicated with A_b increase, which consequently made it difficult to present clear plots of its ensuing behavior. For this reason, from the bubble center positions in X, Y and Z directions, the global motion can be understood (Fig. 7). Understandably, the bubble takes a longer time to arrive at the top when the amplitude increases. From 11s in the no vibration case to 38.5s when A_b = 0.1 m/s^2 (Fig. 7a). With the amplitude increment, the oscillations become intense in both X and Z directions and change the bubble shape that slows down the bubble motion. The bubble oscillates around the Z axis in the first 10s for all the amplitudes, then deviates (Fig. 7b). Regarding the X direction, the oscillations are noticeable from A_b = 0.05 m/s^2. For A_b = 0.06 m/s^2, the bubble oscillations are quite symmetric on the negative side related to the X axis before reaching the top. Beyond A_b = 0.06 m/s^2, those oscillations become asymmetric and drift, displaying a transient behavior (Figs. 4c, 4d). The second oscillation begins with different velocity and shape than the first oscillation and the same thing behavior can be observed for the other oscillations. Additionally similar dynamics have been observed for high frequencies and amplitudes by Movassat et al. (2009). Compared to the frequency variation effects, the amplitude influences considerably not only the bubble trajectory but also the arrival time at the top. In fact, the bubble migration decelerates or accelerates with the frequency increase as compared to a negligible difference vis-à-vis the no vibration case. However, it always decelerates with amplitude augmentation. The influence affecting the shape is greater at high amplitudes caused by the changes that also occur regarding the inertia and pressure forces on the bubble. Therefore, the bubble displays a non-linear behavior while incorporating vibration influences on the thermocapillary force.

Vibration impact on different Ma_T

For f = 0.2 Hz and A_b= 0.005 m/s^2, the temperature of the top is changed from 310 K to 330 K corresponding to Ma_T = 162.7 and Ma_T = 488 respectively. Figure 8 shows different bubble trajectory shapes. The bubble oscillates and its shape deforms while traveling from the bottom to the top. However, in the no vibration case, regardless of Ma_T, the bubble motion keeps a vertical linear trajectory. Furthermore, the bubble takes less time to reach the top whenever the Marangoni number is important (Fig. 9a). Actually, this finding is similar to the results found by Alhendal et al. (2013) for the no vibration

case. Oscillations are also noticed in the Z direction (Fig. 9b). In the X direction, the bubble is in a translatory motion for the first 2.5s when Ma_T = 162.7. Then, oscillations appear drifting to the positive side when the bubble approaches the container top (Fig. 9.c). For Ma_T = 244 and Ma_T = 325.35, the first oscillation is negative then becomes positive, drifting up and finally pushing the bubble to the positive side of the container wall. Beyond those Marangoni numbers, the oscillations are asymmetrical around the X axis and pushing the bubble near the container center. In fact, the undulations, at Ma_T = 162.7, are very noticeable compared to the other cases. In this studied Marangoni range, those undulations diminish with Ma_T increase. Therefore, when the temperature difference is important, the thermocapillary force is less affected by the vibration.

Conclusions

In a container full of ethanol, a nitrogen bubble migration under vibration, in zero gravity environment, is studied using ANSYS/FLUENT. The governing equations of the simulated model are discretized using the finite volume method and solved by the PISO algorithm. The VOF method with the geometric reconstruction scheme is employed to model the two-phase flow. Either changing the amplitude or the frequency, the bubble motion changes from vertical translation to oscillatory trajectories due to the deformations imposed on the bubble shape. For a fixed amplitude and regardless of the frequency, the bubble arrival time is slightly similar to the no vibration case, despite the changes observed on the trajectory. However, when the amplitude increases, asymmetric and drift oscillations are observed making the bubble migration slower vis-à-vis the no vibration case. In general, the motion leading force is the thermocapillary force, but choosing the adequate frequency and amplitude plays an important role in either accelerating or slowing down the bubble migration. Similar to the no vibration case, increasing the Marangoni number accelerates the bubble migration. Those novel results, which are difficult to obtain by experiments, can help researchers to fathom out the thermocapillary flow and bubble motion in space and therefore, enable practices to exploit them in the best way possible in different applications as fluid management and multiphase flows.

Declarations

Funding

No funds, grants, or other support was received from any organization to conduct this work.

Conflict of Interest Statement

The authors declare that there are no financial or proprietary interests that can lead to a conflict of interest in the current paper.

Availability of data and material

The data used to support the findings of this study are included within the article and its supplementary material.

Ethical Statement

All authors have been personally and actively involved in substantive work leading to this manuscript and will hold themselves jointly and individually responsible for its content. They also testify that the article, Thermocapillary Bubble Oscillations and Migration in a Vibrating Cylinder in a Zero-Gravity Environment, submitted to Microgravity Science and Technology Journal has not been published elsewhere and is not currently being considered for publication in another journal.

Consent to participate

All authors are accepting to participate in the following manuscript.

Consent for publication

All authors are giving their consent for publication to their research findings in this manuscript.

Authors' contributions

This manuscript is a continuation of a series of research papers published by Yousuf Alhendal and Ali Turan, three of which have been published in the Journal of Microgravity for Science and Technology. All researchers agreed to search for a new scenario that had not been investigated, and all researchers agreed to study the effect of simple vibrations on the trajectory of bubbles in a zero-gravity environment. Yousuf Alhendal, Sara Touzani, and Abdelkhalek Cheddadi prepared the previous studies and reviewed all references related to this research as well as preparing the sub-code for inclusion in the Ansys Fluent program. Yousuf Alhendal, Ali Turan, and Sara Touzani performed all validation of the results with previous studies and their inclusion in this manuscript. They also wrote the main manuscript text, drew the figures and extracted the results. Abdelkhalek Cheddadi reviewed the paper with the author Ali Turan before sending it for publication in the journal.

References

1. Ahadi, A., Saghir, M. Z.: Experimental study of the impacts forced vibration on thermodiffusion phenomenon in microgravity environment, Appl. Therm. Eng. 60, 348-358 (2013).
2. Alhendal, Y., Turan, A., Hollingsworth, P.:Thermocapillary simulation of single bubble dynamics in zero gravity, Acta Astronaut. 88, 108-115 (2013).
3. Alhendal, Y., Turan, A., Kalendar, A.: Thermocapillary migration of an isolated droplet and interaction of two droplets in zero gravity, Acta Astronaut.126, 265-274 (2016 a).
4. Alhendal, Y., Turan A.: Thermocapillary flow and coalescences of Heterogeneous Bubble Size Diameter in a rotating cylinder: A 3D study, Microgravity Sci. Technol. 28, 639-650 (2016 b).

5. Alhendal, Y., Turan, A., Kalendar, A.: Wall effects on the thermocapillary migration of single gas bubbles in stagnant fluids, Heat Mass Transf. 53, 1315-1326 (2017).
6. Balasubramaniam, R., Lacy, C. E., Woniak, G. Subramanian, R. S.: Thermocapillary migration of bubbles and drops at moderate values of the Marangoni number in reduced gravity, Phys. Fluids. 8(4), 872-880 (1996).
7. Balcazar, N., Oliva, A., Rigola, J.: A level-set method for thermal motion of bubbles and droplets, J. Phys. Conf. Ser.745 (3), 032113 (2016).
8. Bleich, H. H.:Effect of vibrations on the motion of small gas bubbles in a liquid, Jet Propuls. 26(11), 958–964 (1956).
9. Brackbill, J. U., Kothe, D. B., Zemach, C.: A continuum method for modeling surface tension, *J.* Comput. Phys. 100, 335–354 (1992).
10. Colin, C., Riou, X., Fabre, J.: Bubble coalescence in gas–liquid flow at microgravity conditions. Microgravity Sci. Technol. 20(3), 243–246 (2008).
11. Dijkink, R. J., Van der Dennen, J. P., Ohl, C. D., Prosperetti A.: The 'acoustic scallop': a bubble-powered actuator, J. Micromech. Microeng. 16, 1653–1659 (2006).
12. Garrabos, Y., Beysens, D., Lecoutre, C., Dejean, A., Polezhaev, V., Emelianov, V.: Thermoconvectional phenomena induced by vibrations in superctical SF_6 under weightlessness, Phys. Rev. E.75, 056317 (2007).
13. Gupta, A., Kumar, A.: Three dimensional turbulent swirling flow in a cylinder: Experiments and computations, Int. J. Heat Fluid Flow. 28, 249- 261 (2007).
14. Hadland, P. H., Balasubramaniam, R., Wozniak, G., Subramanian, R. S.: Thermocapillary migration of bubbles and drops at moderate to large Marangoni number and moderate Reynolds number in reduced gravity, Exp. Fluids. 26, 240-248 (1999).
15. Herrmann, H., Lopez, J. M., Brady, P., Raessi, M. : Thermocapillary motion of deformable drops and bubbles, Proceedings of the 2008 Summer Program, Center for Turbulence research, USA, 155- 170 (2008).
16. Hirt, C. W., B. D. Nichols.1981. Volume Of fluid (VOF) method for the dynamics of free boundaries, *J. Comput. Phys.*, 39, pp. 201–225.
17. Kalendar, A., Alhendal, Y., Turan, A., Abou-Ziyan, H.: Numerical investigation of the effects of high Reynolds and Marangoni numbers on thermocapillary droplet migration, Microgravity Sci. Technol., 33, 1-14 (2021).
18. Kalichetty, S. S., Sundararajan, T., Pattamatta, A.: Thermocapillary migration and interaction dynamics of droplets in a constricted domain, Phys. Fluids. 31, 022106 (2019).
19. Kawaji, M., Liang, R. Q., Nasr-Esfahany, M., Simic-Stefani, S., Yoda, S.:The effect of small vibrations on Marangoni convection and the free surface of a liquid bridge, Acta Astronaut. 58, 622-632 (2006).
20. Krishna, R., Van Baten, J. M.:Simulating the motion of gas bubbles in a liquid, Nature. 398, 208 (1999).

21. Ma, X., Balasubramaniam, R., Subramanian, R. S.:Numerical simulation of thermocapillary drop motion with internal circulation, Num. Heat Transf. A. 35, 291-309 (1999).
22. Movassat, M., Ashgriz, N., Bussman, M.: Bubble dynamics under forced oscillation in microgravity environment, Proceedings of the ASME 2009 International Mechanical Engineering Congress and Exposition, 9, 1787-1793(2009).
23. Nagasawa, S., Nomura, W., Miyata, Y., Fukuzawa, Y.: Development of numerical simulator for a bubble behavior driven by Marangoni convection in viscous fluid under micro gravity, WIT Trans Modelling Simul. 29, 83-90 (2001).
24. Nas, S., Tryggvason, G.: Computational investigation of the thermal migration of bubbles and drops. In: Proceedings of the ASME Winter Annual Meeting (AMD-174/FED-175), pp 71–83 (1993).
25. Nie, D. M., Qui, L. M., Zhang, X. B.: Bubble Motion under gravity through Lattice Boltzmann Method, Proceedings of the 2015 International Conference on Artificial Intelligence and Industrial Engineering, 123, 531-533 (2015).
26. Nurse, A. K., McFadden, G. B., Coriell, S. R,:Bubble motion and size variation during thermal migration with phase change, Phys. Fluids. 25, 013302 (2013).
27. O'Shaughnessy, S.M., Robinson, A.J.: Numerical investigation of bubble induced marangoni convection: some aspects of bubble geometry. Microgravity Sci. Technol. 20(3), 319–325 (2008).
28. Radulescu, C., Robinson, A.J.: The influence of gravity and confinement on marangoni flow and heat transfer around a bubble in a cavity: a numerical study. Microgravity Sci. Technol. 20(3), 253–259 (2008).
29. Shoikhedbrod, M.: Use a controlled vibration to mixing and separation of a gas bubbles and a liquid under reduced and microgravity conditions, J. Chem. Eng. Process Technol. 7(4), 1000305 (2016).
30. Subramanian, R. S.: Thermocapillary Motion of Bubbles and Drops. In Rath, H. J. (eds) Microgravity Fluid Mechanics, pp. 393-403, Springer, Heidelberg (1992).
31. Thompson, R. L., Dewitt, K. J., Labus. T. L.: Marangoni bubble motion phenomenon in zero gravity, Chem. Eng. Commun. 5, 299-314 (1980).
32. Wang Y., Lu, X., Zhuang, L., Tang, Z., Hu, W.: Numerical simulation of drop Marangoni migration under microgravity, Acta Astronaut. 54, 325-335(2004).
33. Wozniak, G., Balasubramaniam, R., Hadland, P. H., Subramanian, R. S.: Temperature field in a liquid due to the thermocapillary motion of bubbles and drops, *Exp. Fluids* 31, 84-89 (2001).
34. Yamagushi, T., Iguchi, M., Uemura, T.:Behavior of a small single bubble rising in rotating flow field, Exp. Mech. 44, 533–540 (2004).
35. Youngs, D. L.: Time-dependent multi-material flow with large fluid distortion. In K. W. Norton and M. J. Baines, Numerical Methods For Fluid Dynamics, pp. 273–285, Academic Press (1982).
36. Young, N. D., Goldstein, J.S., Block, M. J.:The Motion of Bubbles in a Vertical Temperature Gradient, J. Fluid Mech. 6, 350- 356 (1959).

37. Yu, Z., Yang, H., Fan, L.S.: Numerical simulation of bubble interactions using an adaptive lattice Boltzmann method, Chem. Eng. Sci. 66(14), 3441–3451 (2011).

Figures

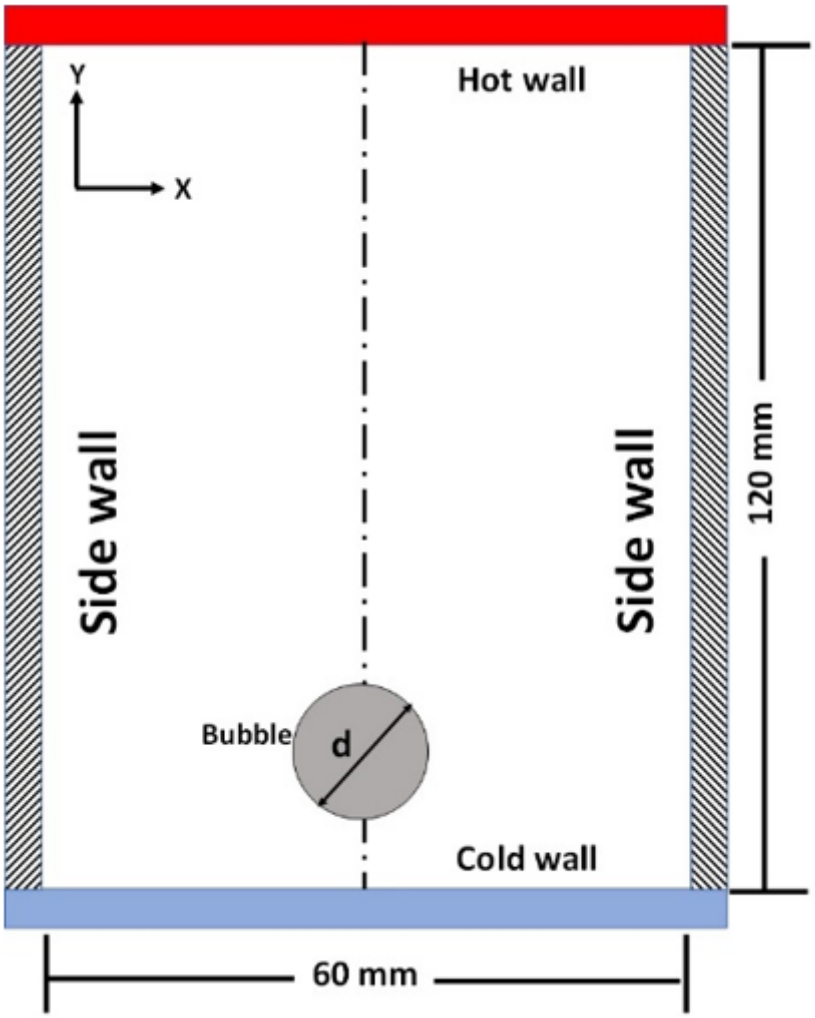

Figure 1

Schematic of the computed field for the bubble migration

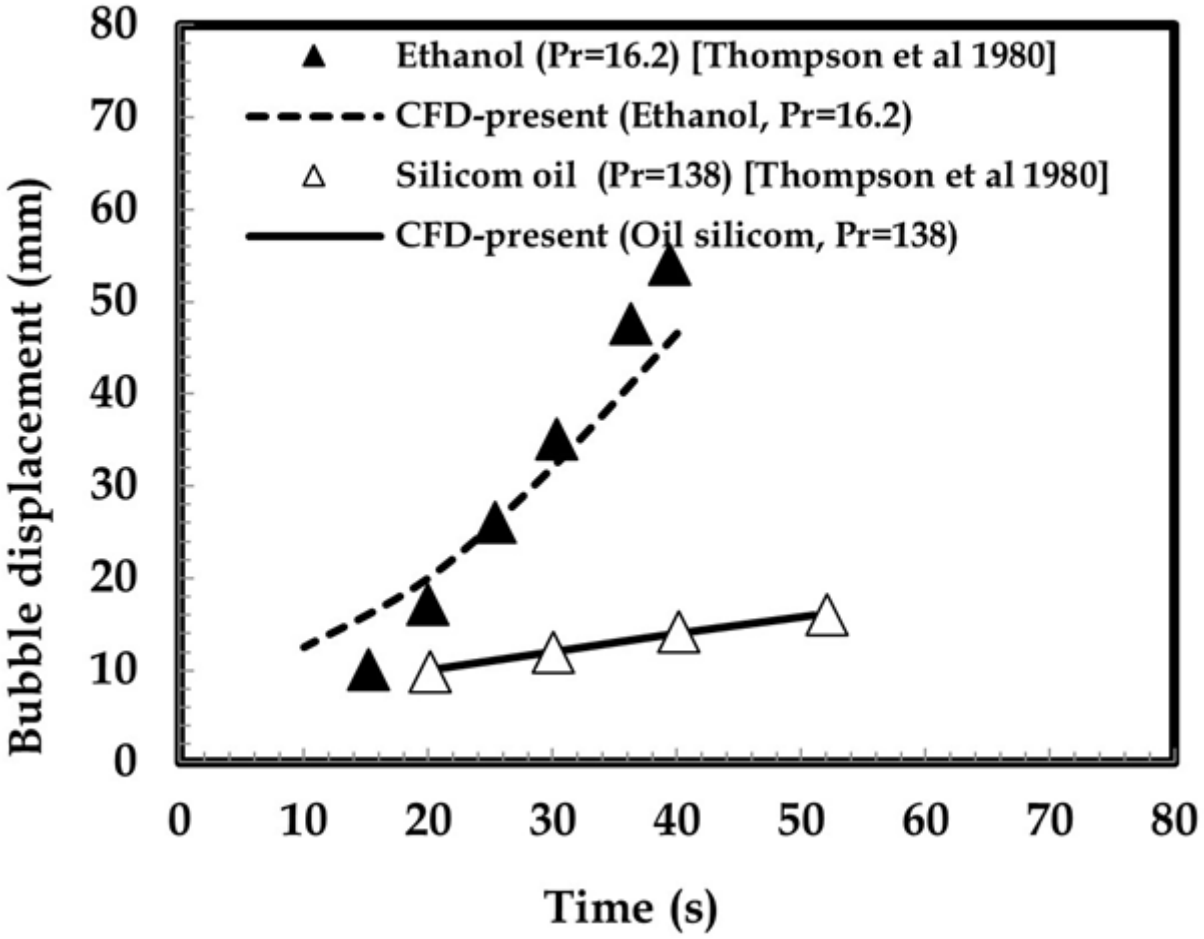

Figure 2

Present results validation with previous work

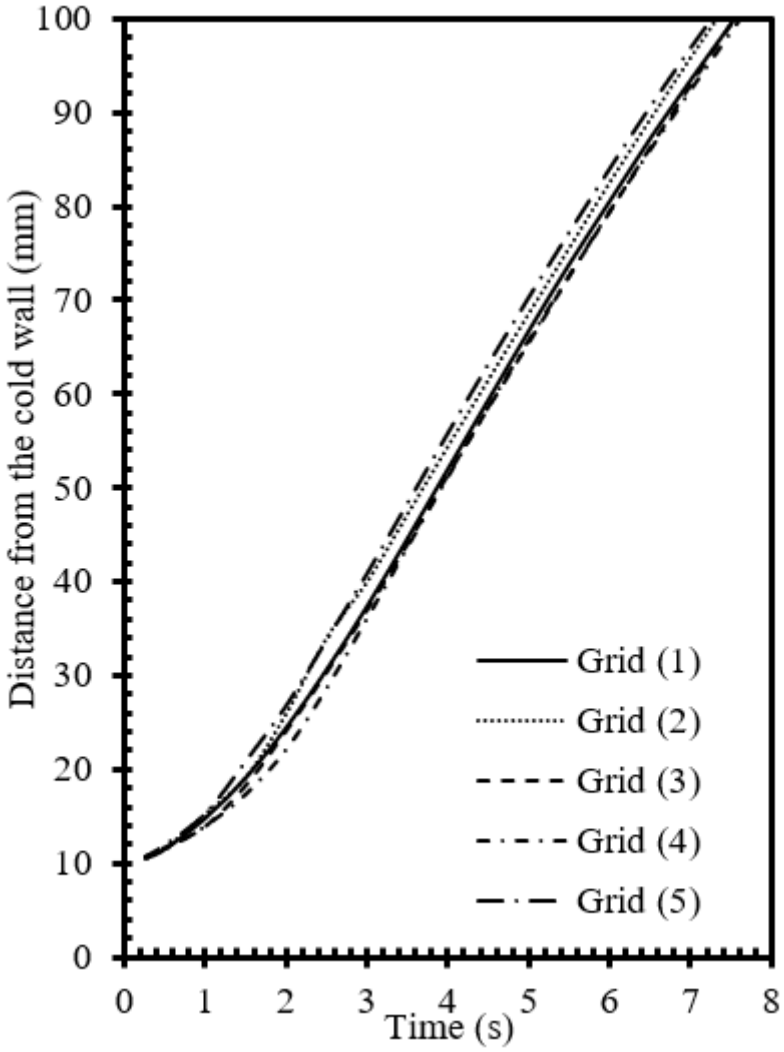

Figure 3

Ascension distance of a bubble nose for five different grid sizes vs. time (s)

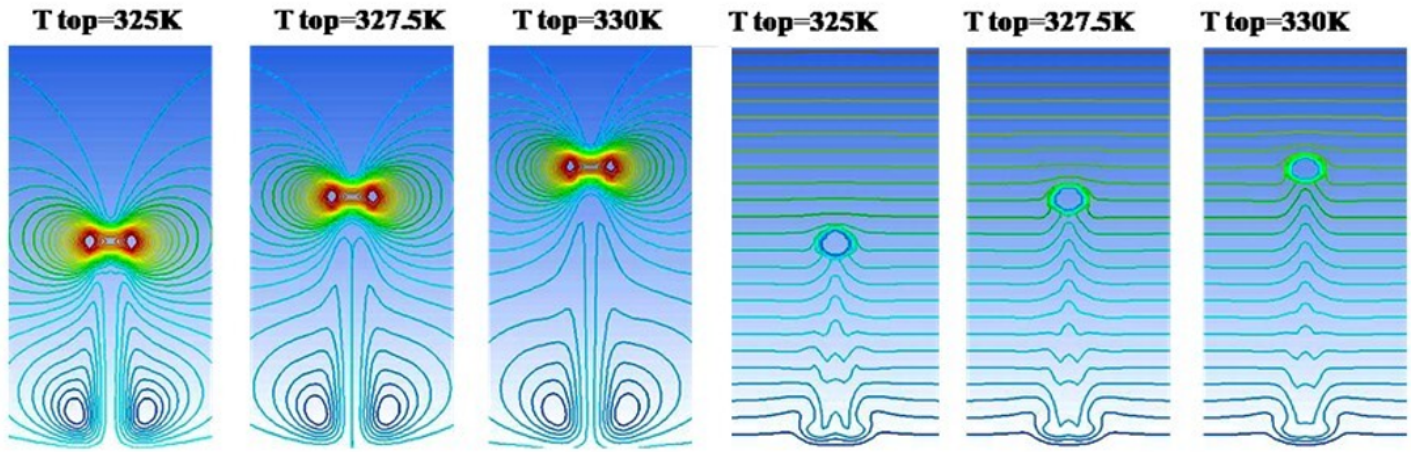

Figure 4

Temperature contours (Right) and streamlines (Left) for the single bubble (d=10 mm) at t=5 s, with bottom wall temperature 300K.

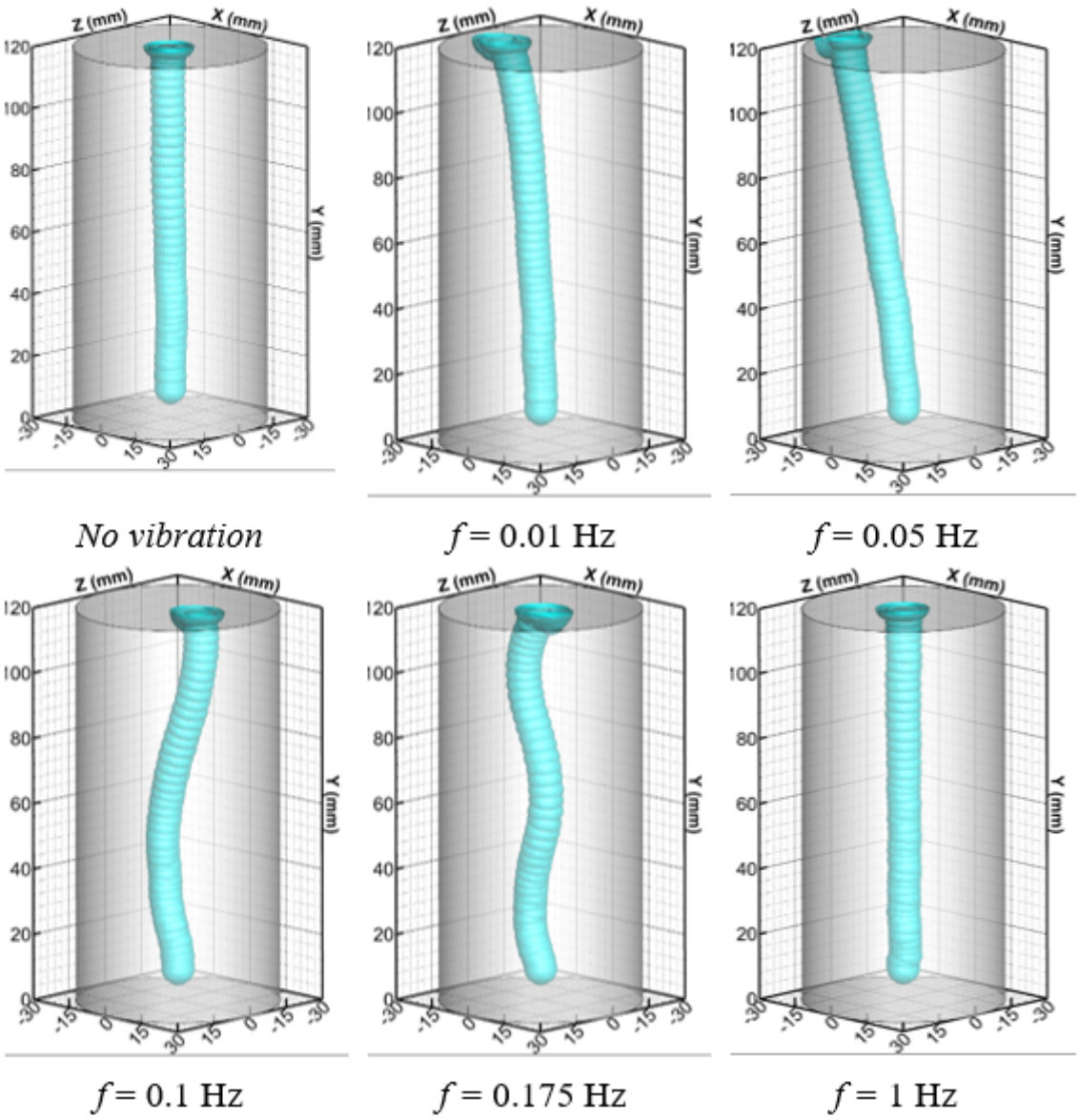

Figure 5

Bubble migration dynamics at different values of vibration frequency for Ma_T = 488 and A_b = 0.005 m/s^2.

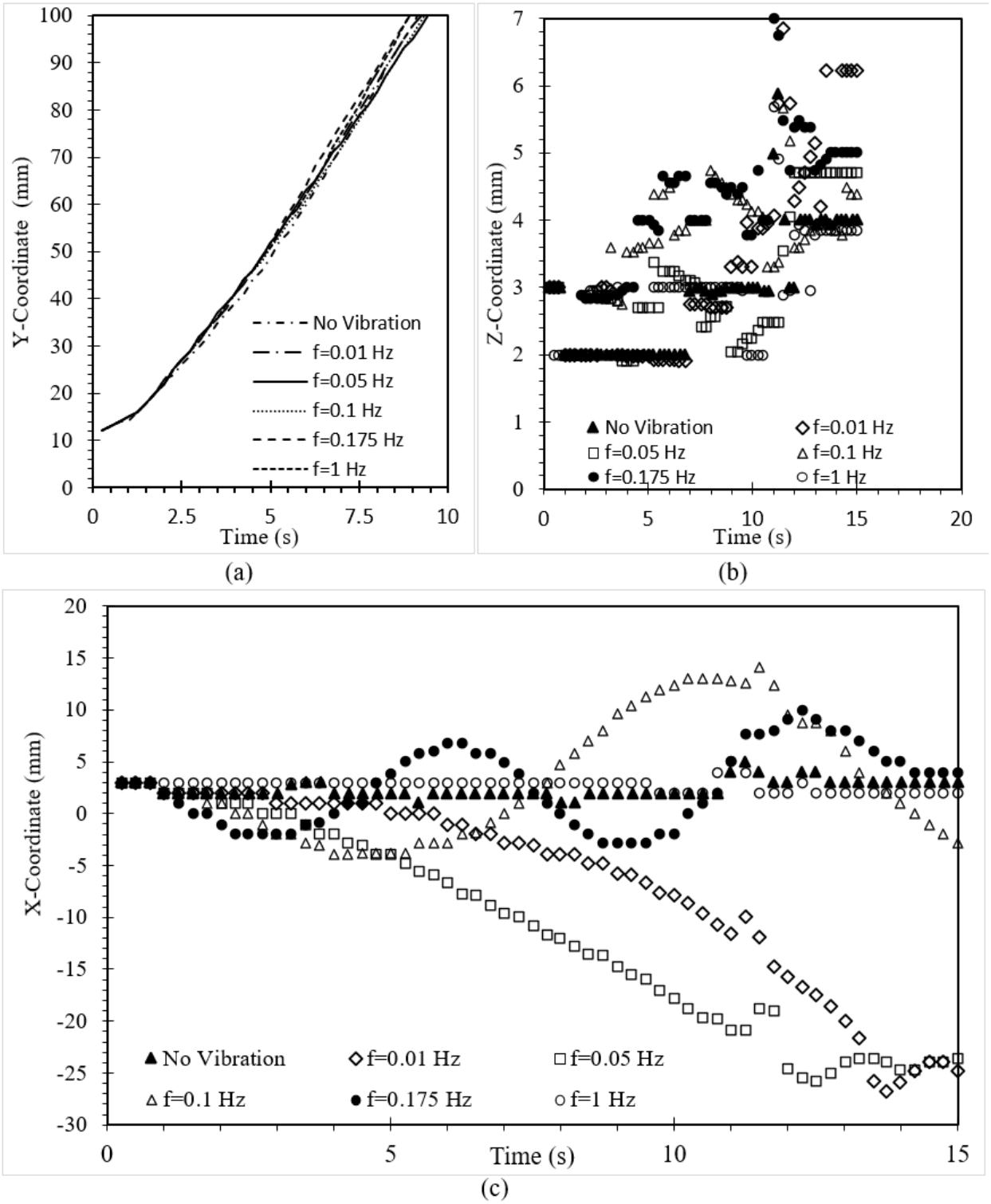

Figure 6

Bubble centre position in the three directions for different frequencies at Ma_T = 488 and A_b = 0.005 m/s^2. (a) Y-direction; (b) Z-direction; (c) X-direction

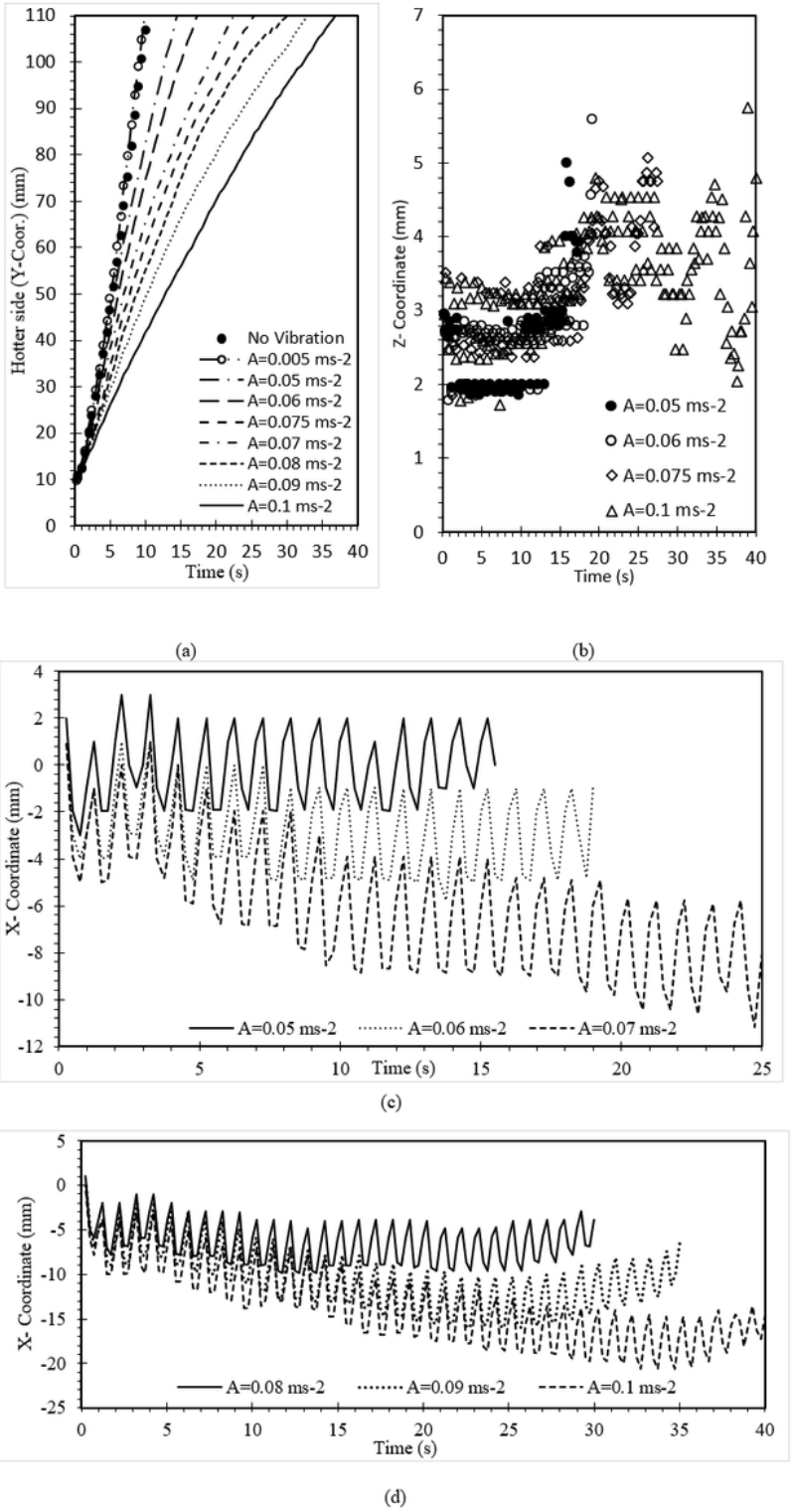

Figure 7

Bubble center position in the three directions for different Amplitudes at Ma_T = 488 and f = 1 Hz. (a) Y-direction; (b) Z-direction; (c) X-direction (0.05,0.06,0.07 ms^{-2}); (d) X-direction (0.08,0.09,0.1ms^{-2}).

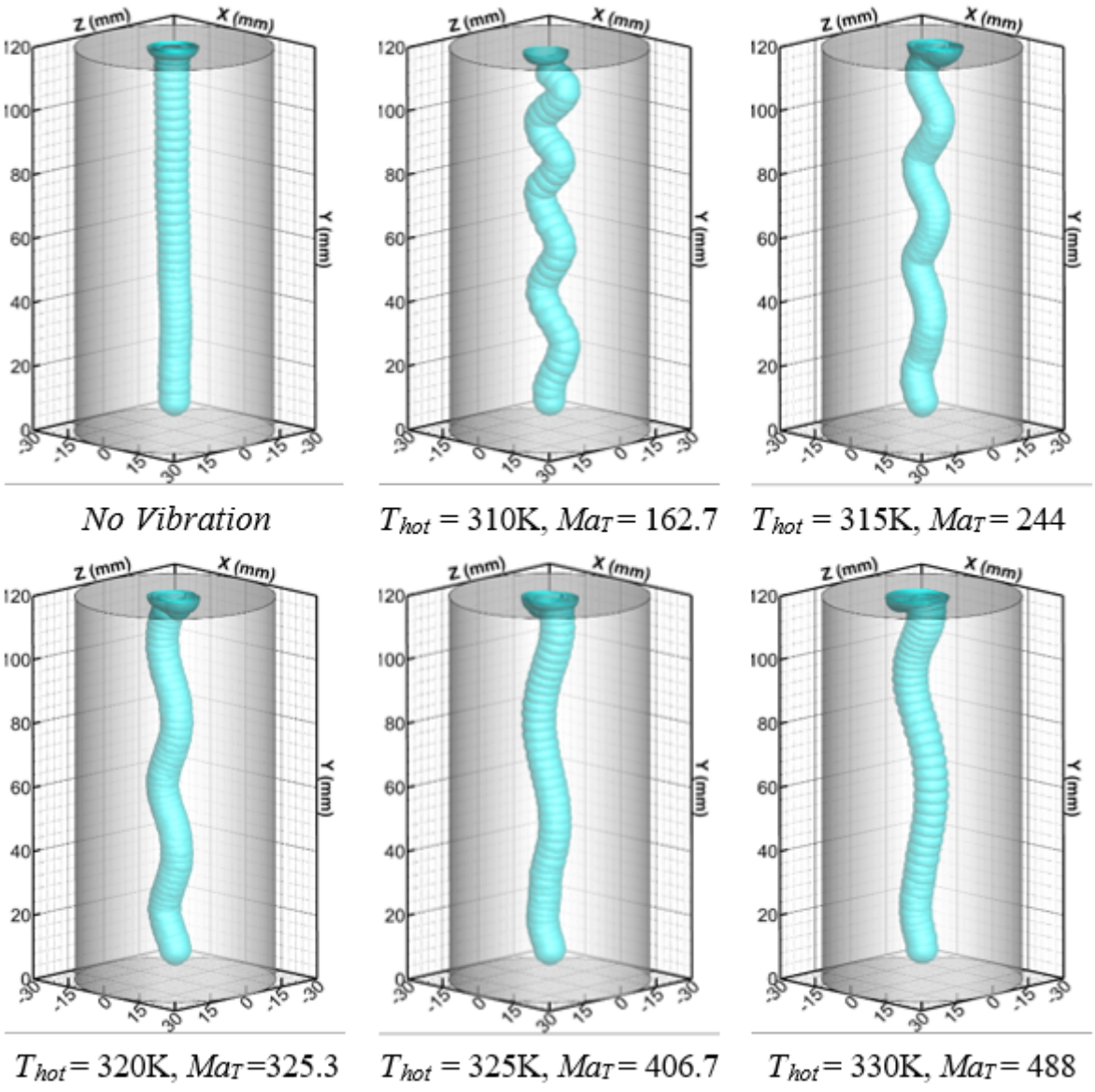

Figure 8

Bubble migration dynamics at different values of Marangoni numbers for f = 0.2 Hz and A_b=0.005 m/s^2.

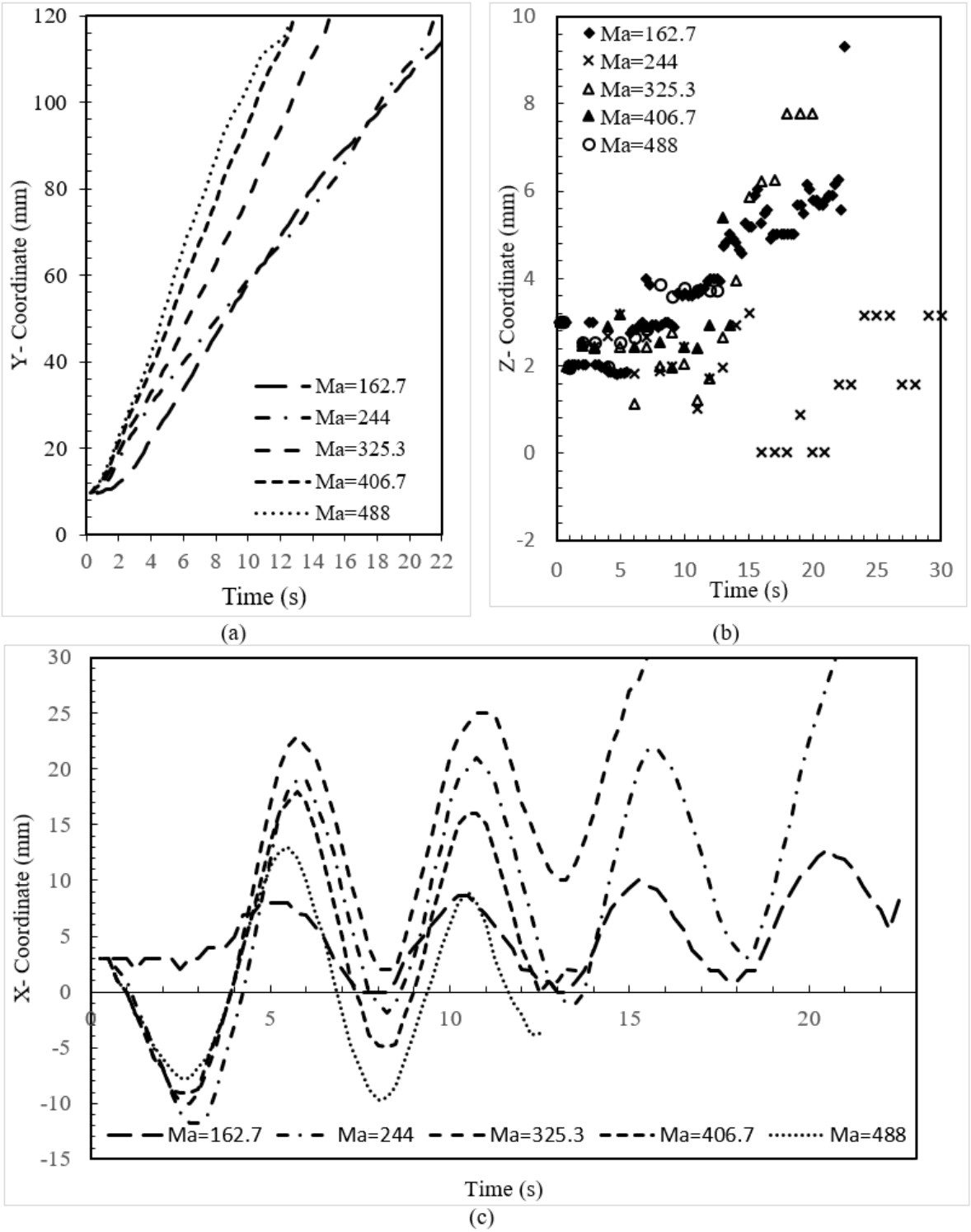

Figure 9

Bubble center position in the three directions for different Ma_T for f = 0.2 Hz and A_b = 0.005 m/s^2. (a) Y-direction; (b) Z-direction; (c) X-direction.